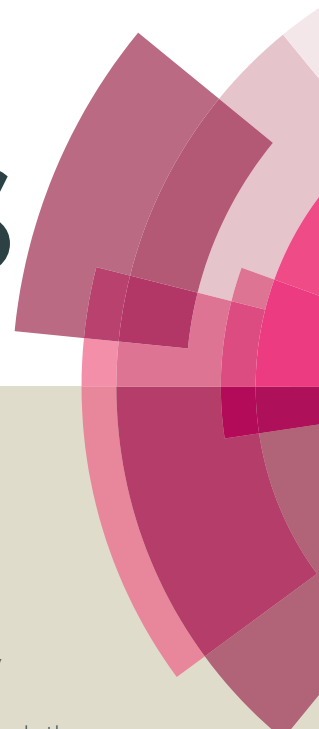


RSC Advances



This article can be cited before page numbers have been issued, to do this please use: Y. Sun, T. Zhou, Q. Pan, X. Zhang and J. Guo, *RSC Adv.*, 2015, DOI: 10.1039/C5RA05769H.



This is an *Accepted Manuscript*, which has been through the Royal Society of Chemistry peer review process and has been accepted for publication.

Accepted Manuscripts are published online shortly after acceptance, before technical editing, formatting and proof reading. Using this free service, authors can make their results available to the community, in citable form, before we publish the edited article. This *Accepted Manuscript* will be replaced by the edited, formatted and paginated article as soon as this is available.

You can find more information about *Accepted Manuscripts* in the [Information for Authors](#).

Please note that technical editing may introduce minor changes to the text and/or graphics, which may alter content. The journal's standard [Terms & Conditions](#) and the [Ethical guidelines](#) still apply. In no event shall the Royal Society of Chemistry be held responsible for any errors or omissions in this *Accepted Manuscript* or any consequences arising from the use of any information it contains.



Journal Name

ARTICLE

PtFe/Nitrogen-doped graphene for high-performance electrooxidation of formic acid with composition sensitive electrocatalytic activity

Yanfang Sun,^{a,b} Ting Zhou,^a Qingyan Pan,^a Xiao Zhang^{a,*} and Jinxue Guo^aReceived 00th January 20xx,
Accepted 00th January 20xx

DOI: 10.1039/x0xx00000x

www.rsc.org/

With the aim to pursue novel high-performance electrocatalysts for fuel cell, a simple synthesis strategy, which consists of hydrothermal reaction followed by solid state reduction by H₂, is developed to prepare a series of Pt_xFe_{100-x}/N-doped graphene nanocomposites with controllable Pt:Fe compositions. The morphology, microstructure, and composition of the samples are systematically characterized with transmission electron microscope, scanning electron microscope, energy dispersive spectroscopy, powder X-ray diffraction, X-ray photoelectron spectroscopy and Raman spectroscopy. The effects of nitrogen doping and alloying with Fe, as well as their synergistic interaction, on the improvement of catalytic performance are well revealed using the present samples as catalysts for formic acid electrooxidation. Additionally, the composition sensitive catalytic activity and stability of these catalysts for formic acid electrooxidation are probed and the optimum Pt:Fe ratio is presented. The optimum sample possesses both the enhanced electrochemical performances and the reduced dosage of noble metal, making it a promising candidate for fuel cell applications.

Introduction

The increasing demands for renewable and clean energy sources with high energy density and low operating temperature have aroused the intensive research interests in the development of high-efficient fuel cells. To satisfy the strict requirement of commercial fuel cells with high current density, electrocatalysts which can high-efficiently oxidize small organic molecules are desired to achieve. Among the high-efficient catalysts of noble metal family, Pt is the preferred catalysts for fuel cells due to its specific catalytic ability to facilitate both the oxidation and reduction reactions.¹ At present, a state-of-art fuel cell requires 0.5 mg Pt per cm² electrode area.² So the production and application of fuel cells require relatively high consumption of Pt, which is scarce and expensive.³ In order to decrease the usage amount of Pt and promote the commercialization of Pt-based fuel cells, the Pt-based catalysts with enhanced catalytic activities are being desired to be achieved. To meet this requirement, two major strategies can be adopted: exploring high-efficient catalysts with lower Pt content and developing novel alternative support materials

with better support performance to replace the traditional carbon black supports due to its bulk structure and low surface area.⁴

As for the first solution, alloying of Pt with another metal M is believed to be an effective way to reduce the consumption of Pt, where M is usually one of the transition metals such as Fe, Co, Ni, Cu, Ti, Pb, Zn, Cd, Hg, Sn, Ru, and Au.⁵⁻²² Demonstrated by the literatures, the addition of transition metals into Pt-based alloy catalysts can not only promote its electrocatalytic activity, but also improve the tolerance to CO poison. On the other hand, graphene has been widely used as the alternative and effective support materials to boost the catalytic performance of Pt, which exhibits unique structure and interesting physical properties such as huge surface area, flexible 2D form, good electrical and thermal conductivities, charge transport mobility, and good chemical stability.^{13-15, 25}

In our previous report, FePt nanoalloys anchored graphene composite has been presented and demonstrated excellent electrocatalytic activity on formic acid and methanol oxidation.⁹ Recently, numerous reports have predicated that, doping graphene with heteroatoms, particularly with N atoms, could effectively tailor its intrinsic electronic characteristics.²⁶⁻²⁹ For instance, the N-doped graphene (NG) shows different spin density and charge distribution compared with the pristine graphene, due to the influence of nitrogen dopants on their neighboring carbon atoms.²⁸⁻³¹ It will introduce "activation region" on the graphene surface, which can participate in catalytic reaction directly and anchor metal nanoparticles used in the catalytic reaction. This kind of material has currently been studied extensively for applications in energy conversion and storage, such as

^aKey Laboratory of Sensor Analysis of Tumor Marker (Ministry of Education), Key Laboratory of Rubber-plastics (Ministry of Education), Laboratory of Inorganic Synthesis and Applied Chemistry, College of Chemistry and Molecular Engineering, Qingdao University of Science and Technology, Qingdao 266042, PR China. Tel: 86 532 84022681; E-mail: zhx1213@126.com (X. Zhang).

^bCollege of Science and Technology, Agricultural University of Hebei, Cangzhou 061100, China.

Electronic Supplementary Information (ESI) available: [details of any supplementary information available should be included here]. See DOI: 10.1039/x0xx00000x

COMMUNICATION

Journal Name

supercapacitors, lithium-ion batteries, and specially oxygen reduction reaction.³²⁻³⁶ So it is worthwhile exploring the influence of NG on the catalytic oxidation activity of Pt-based catalysts for fuel cells.

For fuel cells, liquid phase of formic acid and methanol are two more attractive energy sources than the gaseous or liquid hydrogen due to the ease of handling, transportation and storage.³⁷ In particular, a great deal of research efforts have been focused on direct formic acid fuel cells (DFAFC), because the electrooxidation of formic acid occurs at lower positive potentials than methanol, and the crossover of formic acid through the polymer membrane is lower than that of methanol.^{38,39} Recently, some NG supported Pt-based catalysts have been synthesized and their electrooxidation performance on methanol has been measured,^{20-22, 40, 41} but the studies on formic acid oxidation are rare. Therefore, it would be of great interest to evaluate the electrocatalytic performance of NG supported Pt-based catalysts on formic acids oxidation.

In this manuscript, Pt-Fe alloy nanoparticles anchored on NG sheets are prepared as electrocatalysts for the catalytic oxidation of formic acid. Considering that the alloy composition is also an extremely important factor with respect to the electrocatalytic property,^{11, 42, 43} Pt_xFe_{100-x}/NG catalysts with diverse composition ratios have been presented and the effect of composition on the catalytic activity has been revealed systematically. The results show that, the as-fabricated Pt_xFe_{100-x}/NG catalysts exhibit enhanced electrocatalytic activity on formic acid oxidation and better catalytic stability, due to the contributions from the alloying effect of PtFe and their synergistic interaction with NG sheets. And Pt₄₃Fe₅₇/NG catalyst delivers the highest catalytic activity for formic acid oxidation.

Experimental

Synthesis of graphene oxides

All reagents are obtained from Sinopharm Chemical Reagent Co., Ltd. They are of analytical grade, and are used as purchased without further purification. Graphene oxides (GO) are prepared by oxidizing natural graphite according to a modified Hummers method.⁴⁴ Briefly, graphite powder (2 g) and NaNO₃ (1 g) are added into 50 mL concentrated H₂SO₄ (98%) for 30 min of vigorous stirring under 5 °C. KMnO₄ (0.3 g) is added into the mixture for another 30 min of stirring under 10 °C. KMnO₄ (7 g) is added into the mixture gradually within 1 h, in order to keep the temperature not exceeding 20 °C. Subsequently, the mixture is stirred at 35 ± 5 °C for 2 h to obtain a brown dispersion solution. After 90 mL of distilled water is poured into the dispersion, the temperature is increased quickly and kept above 90 °C for 15 min. Finally, 55 mL of distilled water and 10 mL of 30% H₂O₂ solution are poured into the mixture to terminate the reaction. The resultant light yellow dispersion is filtered, and then is washed with 1 M HCl aqueous solution and a huge amount of distilled water in sequence. The obtained black powders are exfoliated with ultrasonication in water for more than 1 h to prepare

homogeneous brown-black GO dispersion with a concentration of 10 mg mL⁻¹.

Synthesis of catalysts

The synthesis of Pt₇₉Fe₂₁/N-doped graphene composite (Pt₇₉Fe₂₁/NG) can be described as follows: Firstly, 12 mg of K₄Fe(CN)₆·3H₂O and 150 mg of urea are dissolved in 24 mL deionized water. After mixed with 6 mL GO solution (5 mg mL⁻¹), the resultant solution is transferred into a 40 mL autoclave and maintained at 180 °C for 4 h. The products are collected with centrifugation and then washed with absolute ethanol and water in turn for vacuum drying at 60 °C. Subsequently, 60 mg of the hydrothermal products are dispersed in 60 mL H₂PtCl₆·3H₂O solution (0.5 mg mL⁻¹). The dispersion is under ultrasonic irradiation for 30 min and then evaporated at 80 °C under vigorous stirring. Finally, the dried black powders are loaded into a tube furnace and heat-treated at 120 °C for 2 h in H₂/Ar (volume ratio of 5/95) atmosphere with a heating rate of 1 °C min⁻¹ to obtain the final products of Pt₇₉Fe₂₁/NG.

The synthesis procedures of other Pt_xFe_{100-x}/NG catalysts are the same as the preparation of Pt₇₉Fe₂₁/NG except for the different doses of K₄Fe(CN)₆·3H₂O listed in Table 1. For comparison, Pt/NG, PtFe/graphene (PtFe/G), and Pt/G catalysts are prepared via the same synthetic procedure mentioned above by varying the reactants listed in Table 1.

Samples	K ₄ Fe(CN) ₆ ·3H ₂ O	H ₂ PtCl ₆ ·3H ₂ O	Urea
Pt ₇₉ Fe ₂₁ /NG	12	30	150
Pt ₆₀ Fe ₄₀ /NG	39	30	150
Pt ₄₃ Fe ₅₇ /NG	60	30	150
Pt ₂₇ Fe ₇₃ /NG	120	30	150
Pt ₂₀ Fe ₈₀ /NG	180	30	150
Pt ₁₆ Fe ₈₄ /NG	240	30	150
Pt/NG	0	30	150
Pt ₇₉ Fe ₂₁ /G	12	30	0
Pt/G	0	30	0

Table 1 Experimental conditions of different catalysts.

Characterizations of catalysts

The crystal structure of the as-prepared samples is characterized with powder X-ray powder diffraction (XRD, Philips X'pert X-ray diffractometer). Scanning electron microscope (SEM) and energy dispersive spectroscopy (EDS) are recorded with a JEOL JSM-7500F. Transmission electron microscope (TEM) is observed on a JEOL, JEM-2100. Fourier transform infrared (FTIR) spectra are obtained using a Nicolet Magna-IR750. Raman spectroscopy is measured on a confocal microprobe Raman system (LabRam-e010, 632 nm as the excitation source). X-ray photoelectron spectroscopy (XPS) measurements are carried out on a RBD upgraded PHI-5000c ESCA system (Perkin Elmer) with Mg Kα radiation (hν = 1253.6 eV).

Electrochemical measurements

All the electrochemical tests are performed on CHI600D (CH Instruments, Shanghai, China) using a conventional three-electrode cell at room temperature. Modified glassy carbon

electrode (GCE), a saturated calomel electrode (SCE), and a plate wire are used as the working, reference, and counter electrode, respectively. The mixture of 2 mg catalyst, 0.5 mL Nafion solution (0.05wt.%), and 0.5 mL ethanol is ultrasonically dispersed to prepare homogeneous catalyst ink. One portion of catalyst ink (3 μL) is casted on the pretreated GCE surface to fabricate a modified GCE electrode, which is used as working electrode for all electrochemical measurements. The catalytic performances of the catalysts for electrooxidation of formic acid are measured with cyclic voltammograms (CV) technique, which is performed between -0.2 V and 1.2 V at a scan rate of 50 mV s^{-1} in a 0.5 M H_2SO_4 solution containing 1 M HCOOH . Chronoamperometric curves are obtained at a fixed potential of 0.3 V for 10 min. Prior to electrochemical tests, the electrolyte solutions are deaerated by bubbling with N_2 for 15 min.

Results and discussion

Characterization of samples

The as-obtained samples are characterized with TEM techniques. Fig. 1a shows the TEM image of Pt/G composite. Pt particles are aggregated and located unevenly on the surface of graphene sheets with a broad particle size distribution. As shown in Fig. 1b, PtFe alloy particles show larger particle size and deliver worse dispersion states than Pt. On the contrast, the alloy nanoparticles in the case of $\text{Pt}_{79}\text{Fe}_{21}/\text{NG}$ are dispersed uniformly and densely on the NG sheets surface (Fig. 1c). Observed from the magnified TEM image (Fig. 1d), $\text{Pt}_{79}\text{Fe}_{21}$ nanoalloys are monodisperse with a narrow size distribution. The size distribution of PtFe alloy nanoparticles on NG sheets is evaluated statistically by measuring the diameters of two hundred particles from the TEM images and the mean size is around 3.7 nm (inset in Fig. 1c). It is reported that, the nitrogen dopants in the NG sheets can lead to localized defects and promote the graphene chemical activation for enhanced interactions with nanoparticles, thus facilitating their assembly and benefiting their dispersion.^{20-22, 33, 40} Hence, it can be concluded that the improved dispersity of $\text{Pt}_{79}\text{Fe}_{21}$ nanoalloys should be ascribed to the presence of the N-doped sites in the NG sheets, which acts as bonding sites to in situ anchor the nanoparticle precursors.

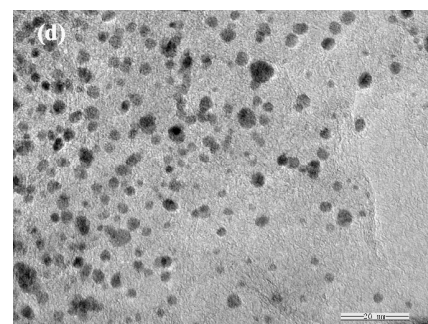
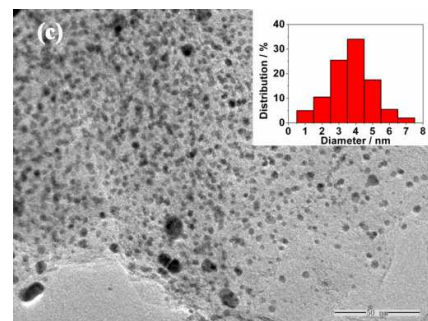
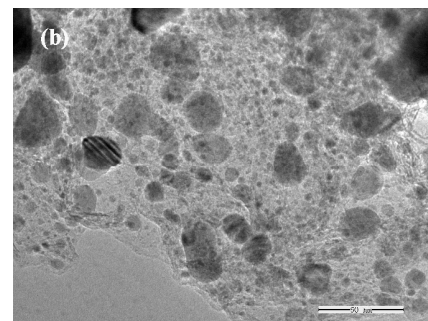
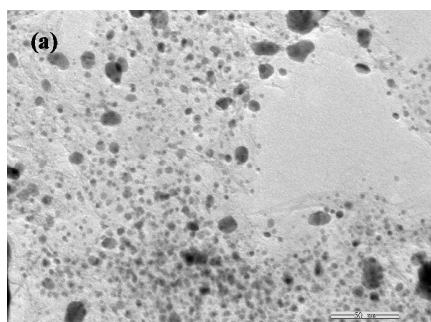


Fig. 1. TEM images of (a) Pt/G, (b) PtFe/G, (c) and (d) $\text{Pt}_{79}\text{Fe}_{21}/\text{NG}$.

The morphology of as-obtained $\text{Pt}_{79}\text{Fe}_{21}/\text{NG}$ catalyst is measured with SEM and is shown in Fig. 2a. The representative wrinkled layer structure of graphene sheets can be observed clearly. EDS is an effective technique to characterize the compositions of composite. As shown in the EDS spectrum of $\text{Pt}_{79}\text{Fe}_{21}/\text{NG}$ (Fig. 2b), Pt, Fe, C, N, and O elements are observed. The Fe and Pt elements can be assigned to the PtFe alloys. The C element corresponds to graphene. The observation of N peak suggests the existence of N element in the composites catalyst. The small amount of O can be ascribed to the residual oxygen-containing functional groups of RGO.⁹ The inset table of Fig. 2b shows that, the weight ratio of C:Pt:Fe:N is determined to be 53.82:26.31:2.08:3.97 with the corresponding atomic ratio of 77.25:2.32:0.64:4.89. The EDS mapping of C, Pt, Fe, and N are presented in Fig. 2c, d, e, and f, respectively. The elements of C and Pt are homogeneously and densely distributed. However, Fe and N elements are distributed evenly and sparsely, which is attributed to their

COMMUNICATION

Journal Name

lower contents. Fig. 2g shows the EDS elemental mapping images of Pt (blue points) and Fe (green points). It can be clearly seen that, the Pt and Fe elements are accompanied with each other, indicating the formation of PtFe alloys. And the NG sheets are almost fully enveloped by the uniformly and densely dispersed PtFe nanoalloys to form a sandwich-like composite structure, which is consistent with the TEM measurement.

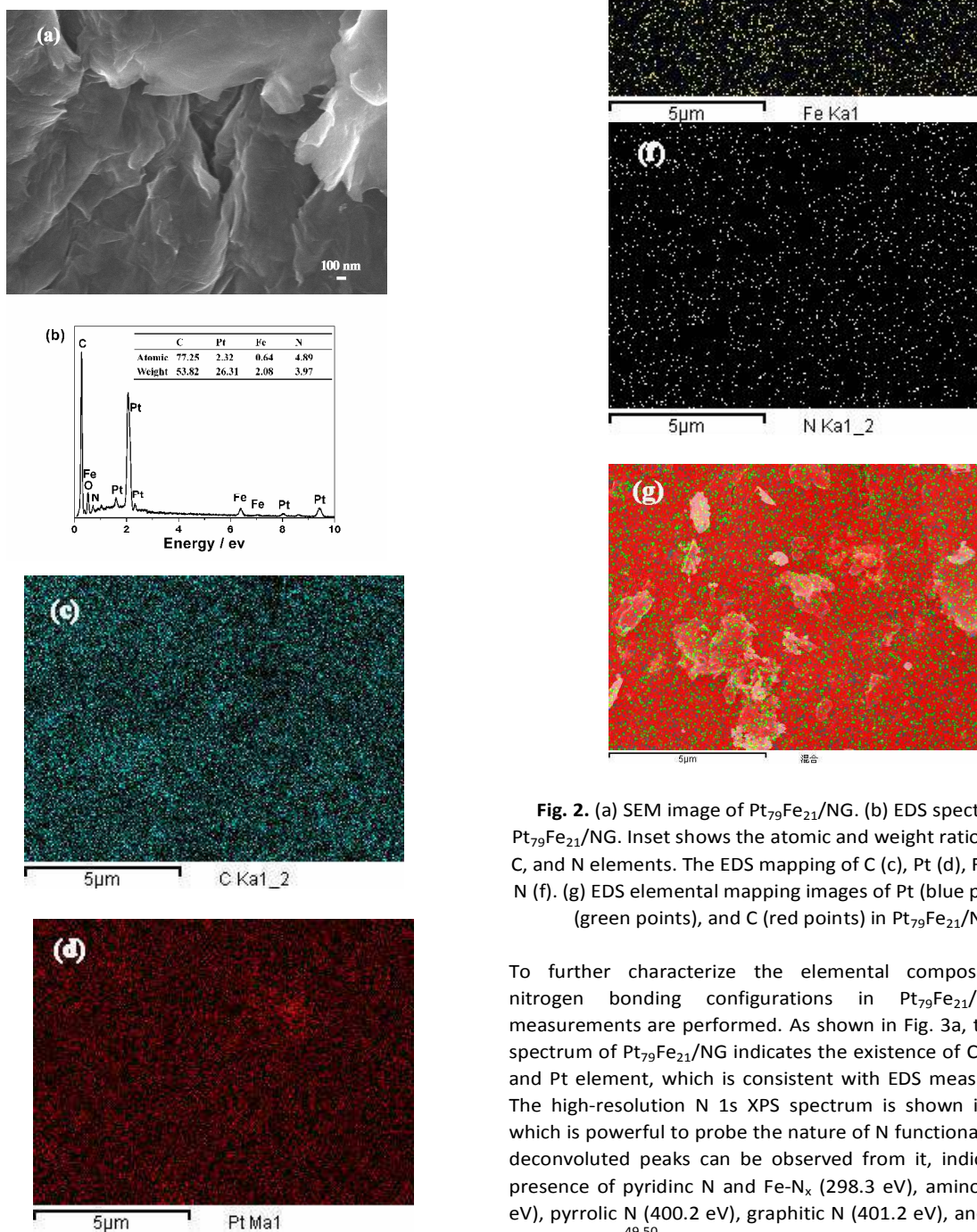


Fig. 2. (a) SEM image of $\text{Pt}_{79}\text{Fe}_{21}/\text{NG}$. (b) EDS spectrum of $\text{Pt}_{79}\text{Fe}_{21}/\text{NG}$. Inset shows the atomic and weight ratio of Fe, Pt, C, and N elements. The EDS mapping of C (c), Pt (d), Fe (e), and N (f). (g) EDS elemental mapping images of Pt (blue points), Fe (green points), and C (red points) in $\text{Pt}_{79}\text{Fe}_{21}/\text{NG}$.

To further characterize the elemental composition and nitrogen bonding configurations in $\text{Pt}_{79}\text{Fe}_{21}/\text{NG}$, XPS measurements are performed. As shown in Fig. 3a, the survey spectrum of $\text{Pt}_{79}\text{Fe}_{21}/\text{NG}$ indicates the existence of C, O, N, Fe, and Pt element, which is consistent with EDS measurements. The high-resolution N 1s XPS spectrum is shown in Fig. 3b, which is powerful to probe the nature of N functionalities. Five deconvoluted peaks can be observed from it, indicating the presence of pyridinic N and Fe- N_x (298.3 eV), amino N (399.2 eV), pyrrolic N (400.2 eV), graphitic N (401.2 eV), and oxidized N (403.0 eV).^{49,50} The existence of Fe- N_x reveals the connection between the doped N and metal Fe, which explains the overlapped elemental mapping of Fe and N, and benefits for

the uniform distribution of alloy nanoparticles on the surface of NG nanosheets. Among these N functionalities, graphitic N, which represents the N atoms doped into the graphitic basal plane, is generally believed to be responsible for the enhanced catalytic activity of N-doped carbon materials.^{26-29,49} Therefore, the presence of graphitic N in Pt₇₉Fe₂₁/NG catalyst will undoubtedly boost its catalytic performance.

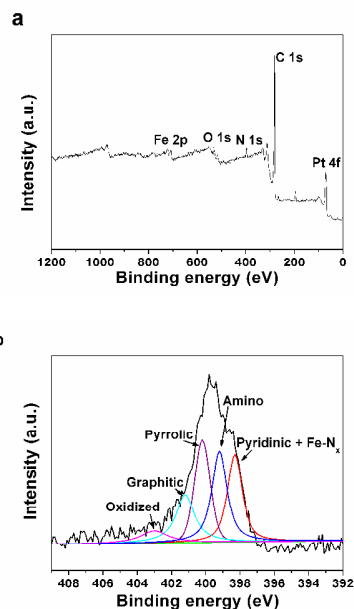


Fig. 3. XPS spectra of Pt₇₉Fe₂₁/NG: (a) survey spectrum and (b) high-resolution N 1s spectra.

The XRD patterns are obtained to determine the composition and crystal structure of the as-prepared GO, NG, Pt/NG and Pt₇₉Fe₂₁/NG. As shown in Fig. 4a, the representative diffraction peak of (001) for GO sheets is observed at 2θ of 9.3°, corresponding to a d-spacing of 0.95 nm. A broad (002) diffraction peak appears at 2θ of ~25.2° in the XRD pattern of NG, indicating that the GO nanosheets have been successfully reduced into NG sheets after the hydrothermal reaction with urea.^{15,45} Besides the NG peak, there are three other peaks at 40°, 46°, and 68° in both Pt/NG and Pt₇₉Fe₂₁/NG nanocomposites, which match well with the (111), (200), and (220) planes of face-centered cubic structure of Pt or PtFe nanoalloys (JCPDS card no. 04-0802). In the XRD pattern of Pt₇₉Fe₂₁/NG, no other impurity peaks according to metallic Fe or its oxides are detected, confirming its high phase purity. Interestingly, in case of Pt₇₉Fe₂₁/NG, the characteristic peaks shift slightly to higher 2θ values with respect to the corresponding peaks in the Pt/NG. Fig. 4b shows the magnified (111) peak in the XRD patterns of Pt/NG and Pt₇₉Fe₂₁/NG. The position of (111) peak of Pt₇₉Fe₂₁/NG locates at higher 2θ value than that of Pt/NG, which can be attributed to the contraction of the lattice constants, indicating the formation of Pt-Fe alloy^{9,15}.

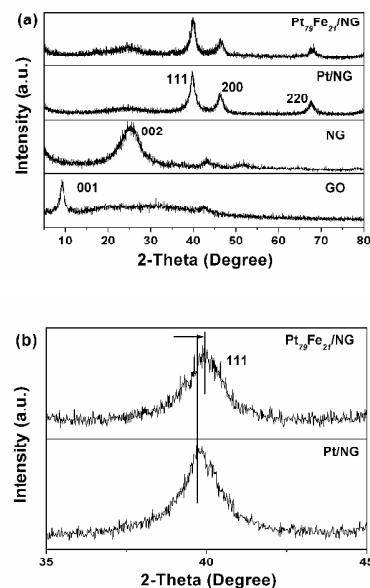


Fig. 4. (a) XRD patterns of GO, NG, Pt/NG and Pt₇₉Fe₂₁/NG; (b) the magnified XRD (111) peak of Pt/NG and Pt₇₉Fe₂₁/NG.

Raman spectroscopy is a very useful tool to characterize structural defects and doping level of graphene.^{20, 22, 28} Fig. 5 shows the Raman spectra of the GO, NG, and Pt₇₉Fe₂₁/NG. Two representative bands of D band (corresponding to structural defects and disorder in graphene) and G band (corresponding to the optical mode vibration of two neighboring carbon atoms) are the predominant features in the spectra of all three samples. Specifically, the intensity ratio of the D and G bands (I_D/I_G) is directly proportional to the defects and can be used to characterize the nitrogen doping in graphene.²⁸ Compared with GO, the NG sheets show a red-shift of D band and an increased I_D/I_G value from 0.94 to 1.12, which should be assigned to the doping of nitrogen into the graphene, as well as the structural and edge defects in graphene. After anchored with PtFe nanoalloys, the Pt₇₉Fe₂₁/NG also displays a slightly red-shifted D band compared with GO due to the nitrogen doping.^{20, 22, 28} And it delivers a further increased I_D/I_G of 1.27, suggesting the interaction between PtFe nanoalloys and NG substrates.⁴⁶

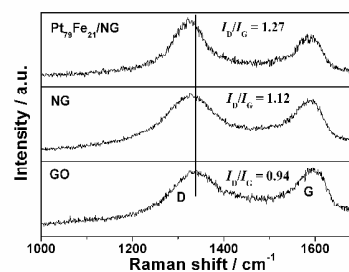


Fig. 5. Raman spectra of the GO, NG, and Pt₇₉Fe₂₁/NG.

Electrochemical measurements

Cyclic voltammograms (CV) recorded for the Pt/G, Pt₇₉Fe₂₁/G, and Pt₇₉Fe₂₁/NG in N₂-saturated 0.5 M H₂SO₄ at a scan rate of 50 mV s⁻¹ are shown in Fig. 6. The pristine graphene and NG electrodes are also tested for comparison. No obvious peak current can be observed for graphene and NG. The other Pt-based samples deliver similar voltammetric features. The typical pair of broad current peaks related to the hydrogen adsorption-desorption are observed between -0.2 and 0.0 V. The anodic peak at about 0.4 V corresponds to the oxidation reaction of Pt (Pt + H₂O → Pt-(OH)_{ad} + H⁺ + e⁻ → Pt-O_{ad} + H⁺ + e⁻). And the reversible reduction reaction of Pt oxides can be observed at about 0.3 V in the cathodic scan. Such voltammetric features have been reported for other Pt based alloys, which can be assigned to the formation of a Pt skin on the catalyst surface.^{9, 22, 42, 47} Among these three kinds of catalysts, Pt₇₉Fe₂₁/NG shows the most prominent reduction peak currents of Pt oxides and hydrogen adsorption-desorption region, which might result from the enhanced synergistic effect between the Pt-Fe alloy and N-G.²² Interestingly, Pt₇₉Fe₂₁/G catalyst shows a slightly positive-shifted reduction peak of Pt oxides in comparison with Pt/G, due to the presence of the alloying element that decreases the desorption free energy of Pt-OH, Pt-O, or Pt-O₂ species. It will lower the adsorption strength of the adsorbed oxygen species on Pt in the alloy and provide more facile oxidation sites of intermediates.⁴⁷ And a further positive shift of the reduction peak is observed for the Pt₇₉Fe₂₁/NG, which should be attributed to the N doping.

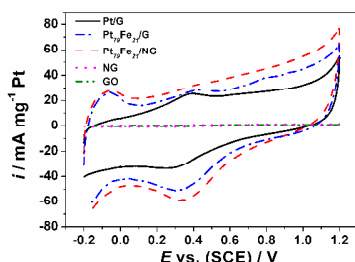
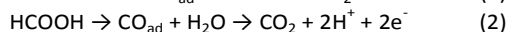
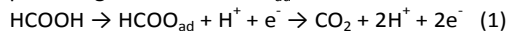


Fig. 6. CV curves of GO, NG, Pt/G, Pt₇₉Fe₂₁/G, and Pt₇₉Fe₂₁/NG catalysts in 0.5 M H₂SO₄.

It is believed that, the doping of nitrogen into graphene could introduce the atomic charge density and asymmetry in the spin density of the graphene network, thus facilitating the charge transfer between the graphene support and the anchoring metals.^{22, 26-31} So when NG is used as the support for Pt-based catalyst, it can evidently enhance the interaction between catalytic metals and carbon substrate, thus improving the catalytic activity for formic acid electrooxidation. With the aim to reveal the enhanced catalytic activity of the presented Pt_xFe_{100-x}/NG catalysts, the electrochemical formic acid oxidation reaction on GO, NG, Pt/G, Pt/NG, Pt₇₉Fe₂₁/G, and Pt₇₉Fe₂₁/NG catalysts is evaluated by recording CV in 0.5 M

H₂SO₄ containing 1 M HCOOH. It is well known that the HCOOH electrooxidation on Pt catalysts usually takes a dual-pathway mechanism: (1) the direct pathway to CO₂ via a dehydrogenation process that involves a reactive intermediate of adsorbed formate (HCOO_{ad}), and (2) the indirect pathway through a dehydration reaction with the formation of the poisoning intermediate CO_{ad}.^{17,43}



Notably, as shown in Fig. 7, there is almost no peak current for graphene and NG modified electrode, suggesting that they show no catalytic activity for formic acid electrooxidation. In contrast with this, all Pt-based catalysts deliver distinct peak current and show similar voltammetric features. Only one peak at around 0.7 V, which corresponds to the oxidation of CO generated by dehydration of HCOOH, is observed during the positive scan of the CV curve.⁴² The oxidation current peak for direct oxidation of HCOOH into CO₂ is indistinct. And the peak corresponding to the oxidation of intermediate species formed during the formic acid oxidation is observed at the negative scan of CV curves. These voltammetric features indicate that formic acid electrooxidation on these catalysts react mainly through the indirect pathway. The oxidation peak current at negative scan of Pt/G is 25 mA mg⁻¹. In contrast with it, Pt/NG (62 mA mg⁻¹) and Pt₇₉Fe₂₁/G (111 mA mg⁻¹) show higher peak current due to the nitrogen doping and alloying with Fe element, respectively. And Pt₇₉Fe₂₁/NG catalyst delivers the highest value of 186 mA mg⁻¹ among these four samples, corresponding to the enhanced synergistic effect between the Pt-Fe alloy and N-G. It is worth noting that, the peaks located at negative scan are observed at ~ 0.27 and 0.29 V for Pt/NG and Pt₇₉Fe₂₁/NG, respectively, while the peaks of Pt/G and Pt₇₉Fe₂₁/G locate at ~ 0.37 and 0.43 V, respectively. This obvious negative shift of the oxidation peak should be assigned to the nitrogen doping, which is beneficial for formic acid electrooxidation. Noting that, the oxidation peak of Pt/NG at negative scan is located at ~ 0.27 V, showing obvious negative shift compared with that of Pt/G, which should be ascribed to the nitrogen doping into graphene. The comparison of peaks position between Pt₇₉Fe₂₁/NG and Pt₇₉Fe₂₁/G also confirms this conclusion. So it can be concluded that, NG substrates can reduce the oxygen potential of the composite catalyst for formic acid indirect electrooxidation, thus improving the catalytic activities of the composite catalyst.

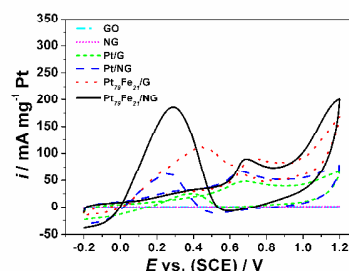


Fig. 7. CV curves of GO, NG, Pt/G, Pt/NG, Pt₇₉Fe₂₁/G, and Pt₇₉Fe₂₁/NG catalysts in 0.5 M H₂SO₄ containing 1 M HCOOH.

Fig. 8 compares the catalytic activity of Pt_xFe_{100-x}/NG catalysts to elucidate the composition sensitive of the formic acid oxidation. Initially, with the increasing Fe composition in the alloy, the oxidation peak current at negative scan increases from 186 mA mg⁻¹ of Pt₇₉Fe₂₁/NG to 421 mA mg⁻¹ of Pt₆₀Fe₄₀/NG and reaches up to the highest value of 603 mA mg⁻¹ for Pt₄₃Fe₅₇/NG, which is ~24 times that of Pt/G. After that, the catalytic activity of Pt_xFe_{100-x}/NG decreases with the further increase of Fe component. The oxidation peak current values are 281 and 97 mA mg⁻¹ for Pt₂₇Fe₇₃/NG and Pt₂₀Fe₈₀/NG, respectively. When the Fe composition increases up to 84%, the as-obtained Pt₁₆Fe₈₄/NG nanocomposites almost show no detectable catalytic activity for formic acid oxidation.

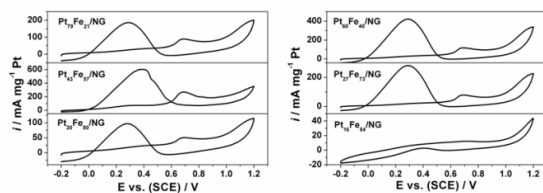


Fig. 8. CV curves of the Pt_xFe_{100-x}/NG catalysts in 0.5 M H₂SO₄ solution containing 1 M HCOOH at a scan rate of 50 mV s⁻¹.

Fig. 9 presents the TEM images of Pt₆₀Fe₄₀/NG, Pt₄₃Fe₅₇/NG, Pt₂₇Fe₇₃/NG, Pt₂₀Fe₈₀/NG, and Pt₁₆Fe₈₄/NG. Except for Pt₁₆Fe₈₄/NG, the alloy nanoparticles in the other four kinds of catalysts are dispersed on the NG sheets with a narrow size distribution, which is similar to that of Pt₇₉Fe₂₁/NG. As for Pt₁₆Fe₈₄/NG, a few large particles are observed, due to the high ratio of Fe element in alloy. So it can be concluded that, the presented Pt_xFe_{100-x}/NG catalysts show obvious composition sensitive activities on formic acid electrooxidation. And the optimum composition of Pt:Fe atomic ratio is obtained at about 1:1 in our presented study. It is believed that, under certain optimum composition, the surface area of Pt skin is maximized to absorb HCOOH and the second metal supplies enough surface sites to promote the effective oxidative removal of poisonous intermediates in Pt-based bimetallic alloy electrocatalysts. This optimum composition ratio is consistent with the previous results for FePt and PtRu catalysts.^{42, 48}

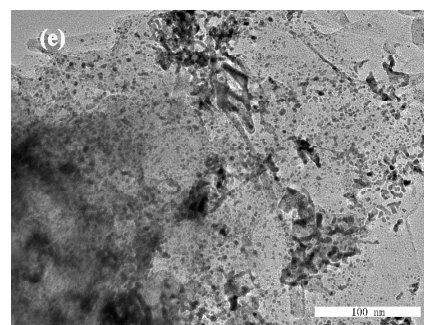
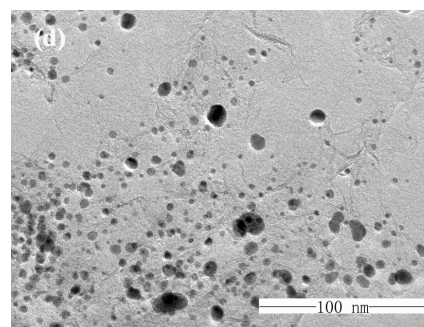
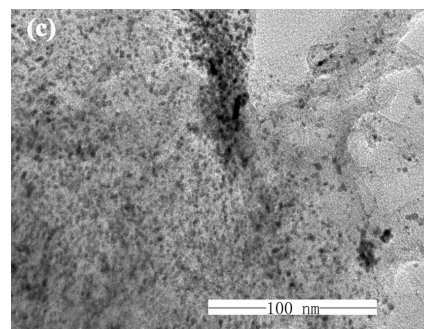
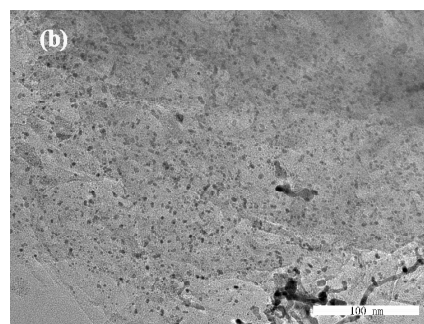
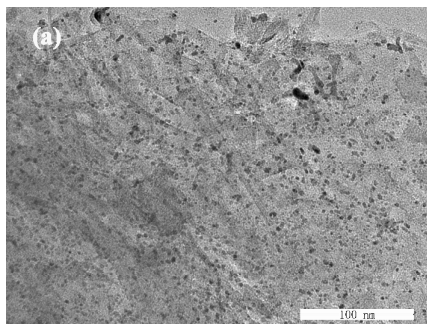


Fig. 9. TEM images of (a) Pt₆₀Fe₄₀/NG, (b) Pt₄₃Fe₅₇/NG, (c) Pt₂₇Fe₇₃/NG, (d) Pt₂₀Fe₈₀/NG, and (e) Pt₁₆Fe₈₄/NG.

To further compare the catalytic activity and durability of Pt_xFe_{100-x}/NG catalysts, Chronoamperometry tests are conducted and shown in Fig. 10. The catalytic performance of graphene and NG are also conducted for comparison. In accordance with the CV results in Fig. 7, graphene and NG

modified electrodes show no catalytic activity for formic acid oxidation. Observed from Fig. 10, the catalytic stability of Pt₁₆Fe₈₄/NG is very poor and only can maintain several seconds. Pt₂₀Fe₈₀/NG delivers similar curve as the results reported in most literatures, which drops rapidly at the primary stage and then decays slowly to a limiting value. As for Pt₇₉Fe₂₁/NG, Pt₆₀Fe₄₀/NG, Pt₄₃Fe₅₇/NG and Pt₂₇Fe₇₃/NG catalysts, the Chronoamperometric curves show an interesting increase at the first stage, and then show analogous features like Pt₂₀Fe₈₀/NG. This exceptional increase should be attributed to the indirect oxidation pathway of formic acid on these catalysts. In the primary oxidation process, the intermediate species have not formed. So the oxidation current density is low. With the reaction of formic acid oxidation going on, the amount of intermediate species rises, thus inducing the increase of current density at the first stage. This result further confirms the indirect oxidation pathway of formic acid on Pt_xFe_{100-x}/NG catalysts. One can see from these curves, Pt₄₃Fe₅₇/NG delivers the highest start current density, which is consistent with the CV tests presented in Fig. 8. But after ~ 200 s, the curve of Pt₄₃Fe₅₇/NG is overlapping with that of Pt₆₀Fe₄₀/NG, suggesting that Pt:Fe atomic ratio of ~ 1:1 seems to be the optimum composition. And the Pt_xFe_{100-x}/NG catalysts show composition sensitive catalytic stability and decrease in the sequence of Pt₄₃Fe₅₇/NG ≈ Pt₆₀Fe₄₀/NG > Pt₂₇Fe₇₃/NG > Pt₇₉Fe₂₁/NG > Pt₂₀Fe₈₀/NG > Pt₁₆Fe₈₄/NG ≈ 0. It is in accordance with the CV results.

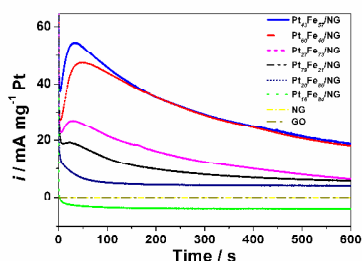


Fig. 10. Chronoamperometric curves of GO, NG, Pt/G and Pt_xFe_{100-x}/NG catalysts in 0.5 M H₂SO₄ solution containing 1 M HCOOH.

Conclusions

In summary, a series of Pt_xFe_{100-x}/NG catalysts have been synthesized via a two-step strategy as catalysts for formic acid electrooxidation. The Pt:Fe ratio can be tuned freely and precisely. The doped nitrogen in graphene supplies additional efficient anchoring sites to deposit metal particles uniformly. The electrochemical tests reveal that, alloying with Fe or using N-doped graphene as supports can evidently enhance the electrocatalytic performance of Pt. The composition sensitive catalytic performance of these catalysts is explored and the optimum composition of Pt:Fe atomic ratio is determined to be 1:1. On the basis of the synergistic interaction between alloy catalysts and NG substrate, the optimum Pt₄₃Fe₅₇/NG catalyst demonstrates amazingly improved electrocatalytic

activity and stability with the reduced dosage of noble metal, making it a promising candidate for fuel cells applications. Moreover, the solutions developed in this manuscript will greatly benefit the rational design and preparation of the high-performance metal catalysts, including Pt or Pd-based catalysts, for small organic molecules oxidation reaction and oxygen reduction reaction.

Acknowledgements

We gratefully acknowledge for the National Natural Science Foundation of China (21003079) and Shandong Provincial Natural Science Foundation, China (ZR2014JL015, ZR2014EMM004).

Notes and references

- H. Zhang, M. Jin and Y. Xia, *Chem. Soc. Rev.*, 2012, **41**, 8035-8049.
- H. A. Grasteiger, D. R. Baker and R. N. Carter, In hydrogen fuel cells: fundamentals and applications. Wiley-CPH, 2010.
- I. E. L. Stephens, A. S. Bondarenko, U. Grønbyerg, J. Rossmeisl and I. Chorkendorff, *Energy Environ. Sci.*, 2012, **5**, 6744-6762.
- M.K. Debe, *Nature*, 2012, **486**, 43-51.
- P. Yu, M. Pemberton and P. Plasse, *J Power Sources*, 2005, **144**, 11-20.
- V. Stamenkovic, B. S. Mun, K. J. J. Mayrhofer, P. N. Ross, N. M. Markovic, J. Rossmeisl, J. Greeley and J. K. Nørskov, *Angew Chem Int Ed*, 2006, **45**, 2897-2901.
- V. R. Stamenkovic, B. S. Mun, M. Arenz, K. J. J. Mayrhofer, C. A. Lucas, G. Wang, P. N. Ross and N. M. Markovic, *Nat. Mater.*, 2007, **6**, 241-247.
- J. Wang, R. M. Asmussen, B. Adams, D. F. Thomas and A. Chen, *Chem. Mater.*, 2009, **21**, 1716-1724.
- J. Guo, Y. Sun, X. Zhang, L. Tang, H. Liu and H. Zhu, *J. Alloys. Compd*, 2014, **604**, 286-291.
- Y. Bing, H. Liu, L. Zhang, D. Ghosh and J. Zhang, *Chem. Soc. Rev.*, 2010, **39**, 2184-2202.
- D. Xu, S. Bliznakov, Z. Liu, J. Fang and N. Dimitrov, *Angew Chem Int Ed*, 2010, **49**, 1282-1285.
- W. Yu, M. D. Porosoff and J. G. Chen, *Chem. Rev.*, 2012, **112**, 5780-5817.
- S. Guo and S. Sun, *J. Am. Chem. Soc.*, 2012, **134**, 2492-2495.
- G. Wei, Y. Zhang, S. Steckbeck, Z. Su and Z. Li, *J. Mater. Chem.*, 2012, **22**, 17190-17195.
- Z. Ji, G. Zhu, X. Shen, H. Zhou, C. Wu and M. Wang, *New J. Chem.*, 2012, **36**, 1774-1780.
- T. Ghosh, Q. Zhou, J. M. Gregoire, R. B. van Dover and F. J. DiSalvo, *J. Phys. Chem. C*, 2010, **114**, 12545-12553.
- B. Habibi and N. Delnavaz, *RSC Adv*, 2012, **2**, 1609-1617.
- Y. Kang, L. Qi, M. Li, R. E. Diaz, D. Su, R. R. Adzic, E. Stach, J. Li and C. B. Murray, *ACS Nano*, 2012, **6**, 2818-2825.
- X. Zhao, J. Zhu, W. Cai, M. Xiao, L. Liang, C. Liu and W. Xing, *RSC Adv*, 2013, **3**, 1763-1767.
- X. Xu, Y. Zhou, J. Lu, X. Tian, H. Zhu and J. Liu, *Electrochim. Acta*, 2014, **120**, 439-451.
- S. Zhao, H. Yin, L. Du, G. Yin, Z. Tang and S. Liu, *J. Mater. Chem. A*, 2014, **2**, 3719-3724.
- G. Yang, Y. Li, R. K. Rana and J. J. Zhu, *J. Mater. Chem. A*, 2013, **1**, 1754-1762.
- V. R. Stamenkovic, B. S. Mun, K. J. J. Mayrhofer, P. N. Ross and N. M. Markovic, *J. Am. Chem. Soc.*, 2006, **128**, 8813-8819.

Journal Name

COMMUNICATION

- 24 G. Krylova, N. M. Dimitrijevic, D. V. Talapin, J. R. Guest, H. Borchert, A. Lobo, T. Rajh and E. V. Shevchenko, *J. Am. Chem. Soc.*, 2010, **132**, 9102-9110.
- 25 N. G. Sahoo, Y. Pan, L. Li and S. H. Chan, *Adv. Mater.* 2012, **24**, 4203-4210.
- 26 L. S. Panchakarla, K. S. Subrahmanyam, S. K. Saha, A. Govindaraj, H. R. Krishnamurthy, U. V. Waghmare and C. N. R. Rao, *Adv. Mater.*, 2009, **21**, 4726-4730.
- 27 J. Liang, Y. Jiao, M. Jaroniec and S. Z. Qiao, *Angew. Chem. Int. Ed.*, 2012, **5**, 111496-11500.
- 28 H. Wang, T. Maiyalagan and X. Wang, *ACS Catal.*, 2012, **2**, 781-794.
- 29 D. Wei, Y. Liu, Y. Wang, H. Zhang, L. Huang and G. Yu, *Nano. Lett.*, 2009, **9**, 1752-1758.
- 30 M. N. Groves, A. S. W. Chan, C. Malardier-Jugroot and M. Jugroot, *Chem. Phys. Lett.*, 2009, **481**, 214-219.
- 31 L. Zhang and Z. Xia, *J. Phys. Chem. C*, 2011, **115**, 11170-11176.
- 32 H. M. Jeong, J. W. Lee, W. H. Shin, Y. J. Choi, H. J. Shin, J. K. Kang and J. W. Choi, *Nano. Lett.*, 2011, **11**, 2472-2477.
- 33 X. Wang, X. Cao, L. Bourgeois, H. Guan, S. Chen, Y. Zhong, D. M. Tang, H. Li, T. Zhai, L. Li, Y. Bando and D. Golberg, *Adv. Funct. Mater.*, 2012, **22**, 2682-2690.
- 34 L. Qu, Y. Liu, J. B. Baek and L. Dai, *ACS Nano*, 2010, **4**, 1321-1326.
- 35 R. I. Jafri, N. Rajalakshmi and S. Ramaprabhu, *J. Mater. Chem.*, 2010, **20**, 7114-7117.
- 36 Y. Zhang, K. Fugane, T. Mori, L. Niu and J. Ye, *J. Mater. Chem.*, 2012, **22**, 6575-6580.
- 37 C. Lamy, A. Lima, V. LeRhun, F. Delime, C. Coutanceau and J. M. Léger, *J. Power Sources*, 2002, **105**, 283-296.
- 38 J. Willsau and J. Heitbaum, *Electrochim. Acta*, 1986, **31**, 943-948.
- 39 Y. W. Rhee, S. Y. Ha and R. I. Masel, *J. Power Sources*, 2003, **117**, 35-38.
- 40 L. S. Zhang, X. Q. Liang, W. G. Song and Z. Y. Wu, *Phys. Chem. Chem. Phys.*, 2010, **12**, 12055-12059.
- 41 X. Xu, Y. Zhou, T. Yuan and Y. Li, *Electrochim. Acta*, 2013, **112**, 587-595.
- 42 W. Chen, J. Kim, S. Sun and S. Chen, *Langmuir*, 2007, **23**, 11303-11310.
- 43 Y. Kim, H. J. Kim, Y. S. Kim, S. M. Choi, M. H. Seo and W. B. Kim, *J. Phys. Chem. C*, 2012, **116**, 18093-18100.
- 44 J. Guo, B. Jiang, X. Zhang, X. Zhou and W. Hou, *J. Solid State Chem.*, 2013, **205**:171-176.
- 45 G. Wang, J. Yang, J. Park, X. Gou, B. Wang, H. Liu and J. Yao, *J. Phys. Chem. C*, 2008, **112**, 8192-8195.
- 46 C. Xu, J. Sun and L. Gao, *J. Mater. Chem.*, 2012, **22**, 975-979.
- 47 K. Zhang, Q. Yue, G. Chen, Y. Zhai, L. Wang, H. Wang, J. Zhao, J. Liu, J. Jia and H. Li, *J. Phys. Chem. C*, 2011, **115**, 379-389.
- 48 H. N. Dinh, X. Ren, F. H. Garzon, P. Zelenay and S. Gottesfeld, *J. Electroanal. Chem.*, 2000, **491**, 222-233.
- 49 Z. Lin, G. H. Waller, Y. Liu, M. Liu and C. P. Wong, *Nano. Energy*, 2013, **2**, 241-248.
- 50 R. B. Hye, S. Jin and S. H. Yang, *Chem. Mater.*, 2011, **23**, 3421-3428.